

## Channeling of Relativistic Laser Pulses, Surface Waves, and Electron Acceleration

N. Naseri,<sup>1</sup> D. Pesme,<sup>1,2</sup> W. Rozmus,<sup>1</sup> and K. Popov<sup>3</sup>

<sup>1</sup>Theoretical Physics Institute, University of Alberta, Edmonton, Alberta, Canada

<sup>2</sup>Centre de Physique Théorique, École Polytechnique, CNRS, 91128 Palaiseau, France

<sup>3</sup>Department of Physics, University of Ottawa, Ottawa, Ontario, Canada

(Received 4 August 2011; published 5 March 2012)

The interaction of a high-energy relativistic laser pulse with an underdense plasma is studied by means of 3-dimensional particle in cell simulations and theoretical analysis. For powers above the threshold for channeling, the laser pulse propagates as a single mode in an electron-free channel during a time of the order of 1 picosecond. The steep laser front gives rise to the excitation of a surface wave along the sharp boundaries of the ion channel. The surface wave first traps electrons at the channel wall and preaccelerates them to relativistic energies. These particles then have enough energy to be further accelerated in a second stage through an interplay between the acceleration due to the betatron resonance and the acceleration caused by the longitudinal part of the surface wave electric field. It is necessary to introduce this two-stage process to explain the large number of high-energy electrons observed in the simulations.

DOI: 10.1103/PhysRevLett.108.105001

PACS numbers: 52.35.Mw, 52.38.Hb

The interaction of high-energy laser pulses at relativistic intensities with underdense plasmas has been an important area of research both for studies of the fundamental aspects of the relativistic laser-plasma interaction physics as well as for physical applications in particle acceleration and radiation sources [1], and in the fast ignition scenario of the inertial confinement fusion [2]. Several experiments, including some very recent ones [3–7], on the propagation of subpicosecond and picosecond pulses in gas jet plasmas have motivated the examination of basic nonlinear physical processes such as relativistic self-focusing [8], laser pulse channeling [9] and channel stability [10,11], surface wakes [12], and the electron acceleration in evacuated channels [13]. All these processes are studied in this Letter by means of 3D particle in cell (PIC) simulations and analytical theory. We will examine the stable laser pulse channeling and a two-stage acceleration process involving the fields of the surface wave (SW) and of the laser beam. First, the surface wave traps electrons at the channel wall and preaccelerates them to relativistic energies; these particles are then energetic enough to be further accelerated in a second stage by an interplay between the betatron resonance [13] and the acceleration by the longitudinal part of the SW electric field. This second stage leads to high-energy gains, well in excess of the ponderomotive potential energy, and to an enhanced number of accelerated electrons in the otherwise electron-free channel.

We consider laser pulses of power  $P_L$  exceeding the critical power  $P_{cr}$  for relativistic self-focusing [9],  $P_L > P_{cr} \equiv [16.2/(n_0/n_c)]GW$ , where  $n_0$  and  $n_c$  denote the electron background density and critical density, respectively. In particular, we will focus our studies on the regime of full electron evacuation from the plasma channel, a process requiring slightly higher laser power, namely,  $P_L > P_{ch} \equiv 1.09P_{cr}$  according to stationary model

predictions [14,15]. The full electron expulsion (or plasma cavitation) has to be considered with particular attention to global charge conservation as was pointed out in Ref. [16] and properly accounted for in 2D [14] and 3D [15] models for a circularly polarized laser light. We have shown before [17] that 2D PIC simulations can reach the stationary states predicted by the model [14]. We found a similar agreement between our 3D PIC simulations and the results of the cylindrically symmetric stationary solutions [15] to the plasma cavitation model [cf. Fig. 1(b)].

The laser beam trapped in the electron-free channel propagates in the  $z$  direction; its normalized electric field  $\vec{E}_L$  is written as  $\vec{E}_L = \frac{1}{2}\{[E_{L\parallel}(\vec{r})\hat{z} + E_{L\perp}(\vec{r})\hat{x}]\exp[-i\{\omega_0(t - z/v_{\phi L})]\} + \text{c.c.}\}$ , where  $\omega_0$  and  $v_{\phi L} \equiv \omega_0/k_{L\parallel} > 0$  denote the laser beam frequency and

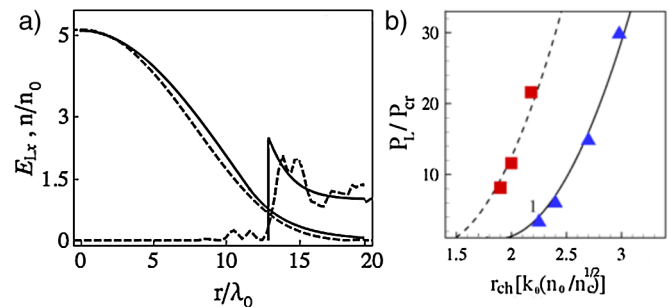


FIG. 1 (color online). (a) Comparison of the theoretical solution for the laser intensity and electron density (solid curves) with the PIC simulation results (dashed curves). The data are taken from the simulation results in the  $y$ - $z$  plane at  $z = 130 \mu\text{m}$  ( $t = 860$  fs). (b)  $P_L/P_{cr}$  as a function of the evacuated channel radius  $r_{ch}k_0(n_0/n_c)^{1/2}$  for linearly (solid curve) and circularly (dashed curve) polarized laser pulses (calculated from the theoretical model). The squares and triangles show the simulation results, “1” refers to the simulation discussed in this paper.

phase velocity, respectively; its parallel wave number, denoted as  $k_{L\parallel}$ , is nonlinearly determined as an eigenvalue of the cavitation model;  $-e$  and  $m\omega_0 c/e$  denote the electron charge and mass, and  $c$  is the speed of light. Throughout our Letter, all the electric field amplitudes  $\vec{E}$  are normalized to  $m\omega_0 c/e$ , i.e.,  $E \equiv e\vec{E}/m\omega_0 c$ . We focus here on the linearly polarized light because of its relevance to experiments [3–5], but our conclusions apply as well to a circularly polarized laser electric field. We modeled the laser beam transverse electric field  $E_{Lx}$  as follows:

$$E_{Lx} = \begin{cases} E_{L_{\max}} J_0(k_{L\perp} r), & r \leq r_{\text{ch}} \\ E_{L_p} K_0(\kappa_{L\perp} r), & r \geq r_{\text{ch}} \end{cases} \quad (1)$$

where  $k_{L\perp} \equiv (k_0^2 - k_{L\parallel}^2)^{1/2}$ ,  $k_0 \equiv \omega_0/c$ ,  $r \equiv \sqrt{x^2 + y^2}$ , and  $E_{L_p} \equiv E_{L_{\max}} J_0(k_{L\perp} r_{\text{ch}})/K_0(\kappa_{L\perp} r_{\text{ch}})$ ;  $r_{\text{ch}}$  denotes the channel radius, so that  $r \leq r_{\text{ch}}$  and  $r \geq r_{\text{ch}}$  correspond to the electron-free channel and to the plasma region, respectively.  $\kappa_{L\perp}$  is determined as a function of  $k_{L\perp}$  from the condition ensuring the continuity of  $E_{Lz}$ , namely,  $\kappa_{L\perp} K_1(\kappa_{L\perp} r_{\text{ch}})/K_0(\kappa_{L\perp} r_{\text{ch}}) = k_{L\perp} J_1(k_{L\perp} r_{\text{ch}})/J_0(k_{L\perp} r_{\text{ch}})$ . The channel radius  $r_{\text{ch}}$  is then determined, following Ref. [15], by the constraint of global charge neutrality:

$$k_0^2 r_{\text{ch}} n_0 / n_c = (E_{L_{\max}})^2 \frac{k_{L\perp} J_0(k_{L\perp} r_{\text{ch}}) J_1(k_{L\perp} r_{\text{ch}})}{[1 + (E_{L_{\max}})^2 J_0^2(k_{L\perp} r_{\text{ch}})/2]^{1/2}}. \quad (2)$$

The above analytical solution to the eigenvalue problem of the laser cavitation corresponds to a linear approximation to the wave equation outside the channel,  $\nabla_{\perp}^2 E_{Lx} - \kappa_{L\perp}^2 E_{Lx} = 0$ , where the field is evanescent. We checked the validity of this approximation in the range of laser intensities corresponding to the condition for a single laser mode propagation,  $P_L < 29.3 P_{\text{ch}}$  [14,15]. This condition, together with  $P_{\text{ch}} < P_L$ , defines the regime of stationary and stable cavitation considered in our Letter, in which electrons are accelerated as discussed further on.

Figure 1(a) compares our model transverse electric field (1) and the electron density in the plasma outside the evacuated channel,  $n/n_0 = 1 + (n_c/n_0)[\nabla^2 \gamma_L/k_0^2]$  ( $\gamma_L^2 \equiv 1 + E_{L_{\max}}^2/2$ ), with the results of 3D PIC simulations that we carried out in Cartesian geometry with the PIC codes MANDOR [18] and SCPIC [19]. The good agreement for the electric field transverse profiles and for the density such as displayed in Fig. 1(a) has been achieved for all the simulations that we carried out in the whole range of laser powers ( $P_{\text{ch}} < P_L < 29.3 P_{\text{ch}}$ ) and for background densities up to  $n_0 = 0.1 n_c$ .

Figure 1(b) displays the location of the stationary states reached in our PIC simulations, for circularly (squares) and linearly (triangles) polarized laser light. They are shown in terms of the trapped laser power,  $P_L/P_{\text{cr}}$ , vs the channel radius  $r_{\text{ch}} k_0 (n_0/n_c)^{1/2}$ . Our PIC simulation results are in very good agreement with the theoretical curves based on the stationary model of Ref. [15]. The specific example of the transverse profiles shown in Fig. 1(a) corresponds to the

background electron density  $n_0 = 10^{-3} n_c$ , the maximum intensity  $I = 5 \times 10^{19}$  W/cm<sup>2</sup>, and the incident pulse full-width-half-maximum  $w_0 = 10$   $\mu\text{m}$ . We have used  $10 \times 10 \times 10$  points per  $\lambda_0^3$  and the total number of particles in the simulation box was about  $7 \times 10^8$ . The laser field is linearly polarized along the  $x$  direction. The laser pulse, of duration  $\tau_p = 400$  fs, propagating along the  $z$  direction, is modeled inside a simulation box ( $200 \times 60 \times 60$   $\mu\text{m}^3$ ) moving with the speed of light. The ions are considered immobile. With these parameters, the laser beam power is  $P_L = 57$  TW, and the ratio  $P_L/P_{\text{ch}}$  is  $P_L/P_{\text{ch}} = 3.3$ , leading to a channel radius  $r_{\text{ch}} = 11.6$   $\mu\text{m}$ .

The characteristic feature of the electron density profile, Fig. 1(a), is its discontinuity at the channel radius  $r_{\text{ch}}$ : the electron density is zero within the channel  $r < r_{\text{ch}}$ , raises to its maximum value at  $r = r_{\text{ch}}$  and quickly decays to the background value for  $r \geq r_{\text{ch}}$ . Such a steep density profile at the channel wall allows the propagation of a SW [12,20]. A rapid growth of a SW is indeed observed in our PIC simulation, as displayed in Fig. 2, which shows the contour plot of the longitudinal component,  $E_z$  [Fig. 2(a)], and transverse component,  $E_y$  [Fig. 2(b)], of the electric field in the  $y$ - $z$  plane, at the time  $t = 860$  fs, (the linearly polarized laser field,  $\vec{E}_{L\perp} \parallel \hat{x}$  has no component in this plane). In Fig. 2(b), it can be clearly seen that, at a given  $y$ , the amplitude of  $E_y$  oscillates as a function of  $z$  with the characteristic wavelength  $\lambda_{\text{SW}} \approx 36$   $\mu\text{m}$  around a nonzero averaged value. These oscillations show that the electric field  $E_y$  is the sum of the  $y$  component of the SW oscillating electric field  $\vec{E}_{\text{sw}} = E_r^{\text{sw}} \hat{r}$  and of the positive charge separation electric field  $\vec{E}_{\text{CS}} = E_r^{\text{CS}} \hat{r}$ , with  $E_r^{\text{CS}} = (n_0/2n_c)k_0 r$  in the electron-free channel, and  $E_r^{\text{CS}} = -\nabla \gamma_L/k_0$  outside the channel. Figures 2(d) and 2(e) show that the PIC simulations results can be very well matched with the analytical solutions for the  $E_z^{\text{SW}}$  and  $E_y^{\text{SW}}$  developed in Ref. [12]. It can also be observed that in addition to oscillations along the  $z$  axis, there is a transverse displacement of the channel wall, showing that the surface wave and the ion channel are unstable with regards to transverse modulations. The combination of these transverse oscillations and of the electron acceleration, as discussed further on, eventually gives rise to the formation of periodic bubble-like structures in place of the evacuated channel, the periodicity and the longitudinal size of the bubbles remaining given by the SW wavelength  $\lambda_{\text{SW}}$ .

The linear theory of SW [12,20] can be easily modified to the case of ion channels and self-trapped laser fields. It should first be noted that in our PIC simulations we observe a single mode characterized by the wave number  $k_{\text{SW}\parallel} \equiv 2\pi/\lambda_{\text{SW}}$ , whereas the SW dispersion relation by itself predicts a continuum of wave numbers for the SW perturbations. This result therefore indicates the existence of a mechanism selecting the SW wave number  $k_{\text{SW}\parallel}$ . We checked that the selecting mechanism is the process described in Ref. [20] and corresponding to the SW re-

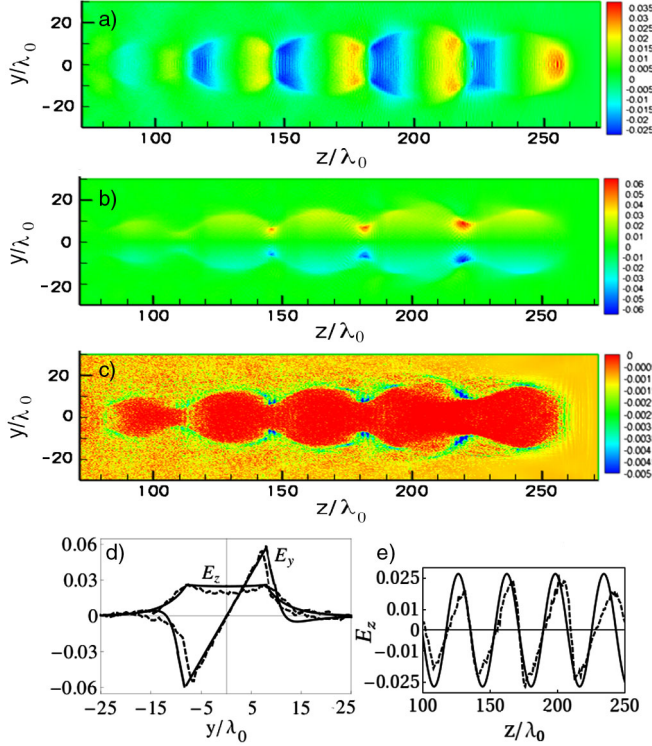


FIG. 2 (color online). Contour plots of  $E_z$  (a),  $E_y$  (b), and electron charge density (c) in the  $y$ - $z$  plane. Comparison of  $E_y$  and  $E_z$  observed in the PIC simulation at  $t = 860$  fs at the cut  $z = 181 \mu\text{m}$  (dashed curves), with the theoretical predictions (solid curves) (d). Similar comparison for  $E_z$ , the cut being taken at  $y = 41 \mu\text{m}$  and  $x = 0$  (e).

sponse to the laser pulse sharp front propagating with the group velocity  $v_{gL}$ : in such a case, the frequency  $\omega_{SW}$  and wave number  $k_{SW\parallel}$  of the SW excited by the laser wave front are solutions to the SW dispersion relation  $D_{SW}(\omega_{SW}, k_{SW}) = 0$  and to the implicit equation  $\omega_{SW} - k_{SW}v_{gL} = \omega_0 - k_0v_{gL}$ . Using a linear description for the propagating front of the laser pulse, the two equations above lead to the solution  $\lambda_{SW}/\lambda_0 = 36$ , in excellent agreement with our simulation results. In addition, it also makes it possible to write the following relation for the SW phase velocity:  $v_\phi^{SW} \equiv \omega_{SW}/k_{SW}$ ,  $v_\phi^{SW} = v_{gL} - (\lambda_{SW}/\lambda_0)(v_{\phi L} - v_{gL})$ , where  $v_{\phi L}$  denotes the laser wave phase velocity. Within the same linear approximation for the laser pulse front, one obtains  $v_\phi^{SW}/c = v_{gL}/c - \lambda_{SW}n_0v_{\phi L}/(\lambda_0n_c c)$ , which leads, for our parameters, to  $v_\phi^{SW}/c = 0.96$ , corresponding to the relativistic  $\gamma$  factor  $\gamma_\phi^{SW} \approx 3$ .

We compared this prediction with our PIC simulation results: by measuring the SW frequency  $\omega_{SW}$ , we were able to determine the SW phase velocity, obtaining  $v_\phi^{SW} \approx 0.95c$  and corresponding to the same  $\gamma$  factor  $\gamma_\phi^{SW} \approx 3$ . Thus, the PIC results are all close to the theoretical predictions, therefore confirming that the process selecting

the SW wavelength is the mechanism described in Ref. [20].

Figure 3 displays the distribution function of the fast electrons, clearly showing a tail formation, with a significant number of fast electrons having their  $\gamma_z \equiv p_z/mc$  in the range  $[40, 200]$ ,  $p_z$  denoting the  $z$  component of the electron momentum  $\vec{p}$ . At the time  $t = 1.9$  ps the distribution function contains a charge of 49.2 nC of electrons having their  $\gamma$  factor larger than 50. The inset in Fig. 3 represents the  $\gamma_z$  factor as a function of the longitudinal coordinate  $z$ . It can be seen that the accelerated electrons form periodic bunches whose periodicity length is the SW wavelength  $\lambda_{SW}$ .

We now investigate the physical origin of these fast electrons. First of all, the SW is able, by itself, to trap and accelerate electrons along the  $z$  direction because of its longitudinal field component  $E_z^{SW}$  [cf. Fig. 2(e)]. This field exists throughout the electron-free channel and on the channel's wall, i.e., in the region of high electron density. From the maximum of the SW electric field  $z$ -component amplitude  $E_z^{SW} \approx 0.03$ , one may compute the largest  $\gamma$  factor, denoted as  $\gamma_{z\max}^{SW}$ , which an initially low energy electron could gain by being trapped along the  $z$  direction in the surface wave [21];  $\gamma_{z\max}^{SW}$  is given by  $(\gamma_{z\max}^{SW})^2 = \gamma_L^2 + p_M^2$ , with  $\gamma_L^2 = 1 + E_{L\max}^2/2$  and where  $p_M$  denotes the maximum normalized electron momentum in the surface wave that corresponds to the potential well  $\Delta\Phi \equiv \Phi_{\max} - \Phi_{\min} \approx 2E_z^{SW}/k_{SW\parallel}$ . We obtain  $p_M \approx 46$  in the case of a normalized electric field amplitude  $E_z^{SW}$  as large as  $E_z^{SW} = 0.03$ , leading to  $\gamma_{z\max}^{SW} \approx 47$ , that is significantly below the  $\gamma$  factors in the range 50, 200 observed in the PIC simulations (Fig. 3). We may therefore *a priori* conclude

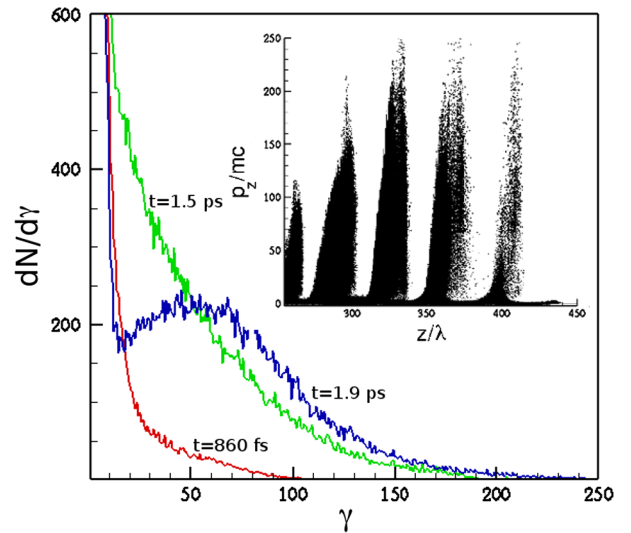


FIG. 3 (color online). Electron distribution function in the simulation box at  $t = 860$  fs, 1.5 ps, 1.9 ps. The inset shows the quantity  $p_z/mc$  as a function of  $z$ , such as observed in the PIC simulation at the time  $t = 1.5$  ps.

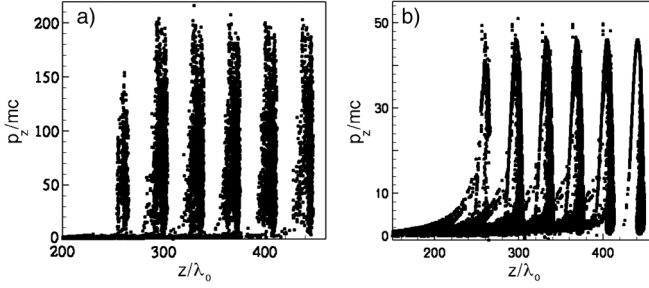


FIG. 4.  $p_z/mc$  vs  $z$  from test particle code for all fields (a), and when only the surface wave is present (b).

that the origin of the fast electrons cannot be reduced to the simple acceleration by the surface wave electric field.

In order to find out the mechanism responsible for the observed fast electrons, we performed several test particles calculations by solving the equations of motion  $d\vec{p}/dt = -(e/m)[\vec{E} + \vec{v} \times \vec{B}]$  for prescribed electric and magnetic fields, including the laser electric field  $\vec{E}_L$  such as that given by Eq. (1), the charge separation field  $\vec{E}_{CS}$  of the evacuated ion channels, and the SW electric field  $\vec{E}_{SW} = E_z^{SW}\hat{z} + E_r^{SW}\hat{r}$  such as that given by the model from Ref. [12]. The longitudinal component of the laser field  $E_{Lz}$  is given by the divergence-free condition  $\vec{\nabla} \cdot \vec{E}_L = 0$ , and the magnetic fields  $\vec{B}$  are calculated from the Maxwell equations. The comparisons between these fields and the PIC results are excellent as it can be seen in Figs. 2(d) and 2(e). We first checked that we correctly recover all the features observed in the PIC simulations, namely, the periodic bunching of the fast electrons with  $\gamma$  factors as large as 200 when all the fields are included into the equations of motion; see Fig. 4(a), which is compared with Fig. 3 at  $t = 1.5$  ps. We also verified that the SW alone is not able to accelerate electrons to energies as high as  $\gamma_z = 200$ : indeed, when only keeping the SW electric field, we obtained electron energies no larger than  $\gamma \leq 50$  (see Fig. 4(b)) consistently with the trapped electron dynamics discussed above.

We then considered the standard betatron acceleration mechanism [13,22]. This mechanism corresponds to a resonance between the motion caused by the laser fields and the transverse oscillation induced by a stationary transverse electric field; in our case, it corresponds to retaining only the charge separation field  $\vec{E}_{CS}$  in addition to the laser fields. As the betatron resonance may occur only if the electron velocity is large enough, the test electrons were introduced initially with the energy  $\gamma_z \approx 50$ ; their maximum final energy corresponded to  $\gamma_z = 140$ , i.e., still significantly smaller than the  $\gamma_z \approx 200$  observed in the PIC simulations. Thus, the standard betatron effect by itself cannot explain our PIC results.

Finally, we combined the betatron process caused by the laser fields and the charge separation field  $\vec{E}_{CS}$  with the acceleration by the longitudinal SW electric field  $E_z^{SW}$ . By doing so, we obtained periodic bunches of fast electrons

having their  $\gamma_z$  factors as large as  $\gamma_z = 200$ , independently of the initial energy of test particles. Therefore, we may conclude that the origin of the fast electrons observed in our PIC simulations is the betatron effect assisted by the parallel acceleration due to the longitudinal SW electric field.

In conclusion, we studied the cavitation of relativistic laser pulses in underdense plasmas. The electron-free channel predicted by the nonlinear stationary model of relativistic self-focusing [15] has been observed in our 3D PIC simulations. In the regime of a single laser mode propagation, the nonlinear channel is stable for a time long enough to support the growth and the propagation of a surface wave. A surface wave, with the wavelength  $\lambda_{SW}$  predicted by Ref. [20], grows quickly in time in response to the steep front of the laser pulse. This surface wave plays a central role in the electron acceleration, first by trapping and preaccelerating a large number of electrons, and then through an interplay between the acceleration caused by the longitudinal component of its electric field and the acceleration due to the betatron resonance [13]. This theoretical scenario should govern the propagation of high-energy short laser pulses in gas jet targets, e.g., Ref. [3].

The authors would like to acknowledge support from the Natural Sciences and Engineering Research Council of Canada. Also N. Naseri would like to thank Abdorreza Samarbakhsh for valuable discussions.

- 
- [1] E. Esarey, C. B. Schroeder, and W. P. Leemans, *Rev. Mod. Phys.* **81**, 1229 (2009).
  - [2] M. Tabak *et al.*, *Phys. Plasmas* **1**, 1626 (1994).
  - [3] L. Willingale *et al.*, *Phys. Rev. Lett.* **106**, 105002 (2011).
  - [4] P. M. Nilson *et al.*, *New J. Phys.* **12**, 045014 (2010).
  - [5] S. P. D. Mangles *et al.*, *Phys. Rev. Lett.* **94**, 245001 (2005).
  - [6] Z. Najmudin *et al.*, *Phys. Plasmas* **10**, 438 (2003).
  - [7] M. Borghesi *et al.*, *Phys. Rev. Lett.* **78**, 879 (1997).
  - [8] A. G. Litvak, *Sov. Phys. JETP* **30**, 344 (1970).
  - [9] G. Z. Sun *et al.*, *Phys. Fluids* **30**, 526 (1987).
  - [10] A. B. Borisov *et al.*, *Plasma Phys. Controlled Fusion* **37**, 569 (1995).
  - [11] V. I. Berezhiani *et al.*, *Phys. Rev. E* **65**, 046415 (2002).
  - [12] T. C. Chiou *et al.*, *Phys. Plasmas* **2**, 310 (1995).
  - [13] A. Pukhov, Z.-M. Sheng, and J. Meyer-ter-Vehn, *Phys. Plasmas* **6**, 2847 (1999).
  - [14] F. Cattani *et al.*, *Phys. Rev. E* **64**, 016412 (2001).
  - [15] A. Kim *et al.*, *Phys. Rev. E* **65**, 036416 (2002).
  - [16] M. D. Feit *et al.*, *Phys. Rev. E* **57**, 7122 (1998).
  - [17] N. Naseri, S. G. Bochkarev, and W. Rozmus, *Phys. Plasmas* **17**, 033107 (2010).
  - [18] D. Romanov *et al.*, *Phys. Rev. Lett.* **93**, 215004 (2004).
  - [19] K. I. Popov *et al.*, *Phys. Plasmas* **16**, 053106 (2009).
  - [20] N. M. Naumova *et al.*, *Phys. Plasmas* **8**, 4149 (2001).
  - [21] C. B. Schroeder *et al.*, *Phys. Plasmas* **13**, 033103 (2006); E. Esarey and M. Pilloff, *Phys. Plasmas* **2**, 1432 (1995).
  - [22] G. D. Tsakiris, C. Gahn, and V. K. Tripathi, *Phys. Plasmas* **7**, 3017 (2000).